Demagnetization of magnetically shielded rooms

F. Thiel, A. Schnabel, S. Knappe-Grüneberg, D. Stollfuß, and M. Burghoff
Physikalisch-Technische Bundesanstalt (PTB), Braunschweig and Berlin, FB 8.2 Biosignals, Abbestrasse 2-12, 10587 Berlin, Germany

(Received 1 December 2006; accepted 8 February 2007; published online 19 March 2007)

Magnetically shielded rooms for specific high resolution physiological measurements exploiting the magnetic field, e.g., of the brain (dc-magnetoencephalograpy), low-field NMR, or magnetic marker monitoring, need to be reproducibly demagnetized to achieve reliable measurement conditions. We propose a theoretical, experimental, and instrumental base whereupon the parameters which affect the quality of the demagnetization process are described and how they have to be handled. It is demonstrated how conventional demagnetization equipment could be improved to achieve reproducible conditions. The interrelations between the residual field and the variability at the end of the demagnetization process are explained on the basis of the physics of ferromagnetism and our theoretical predictions are evaluated experimentally. © *2007 American Institute of Physics.* [DOI: 10.1063/1.2713433]

I. INTRODUCTION

Magnetically shielded rooms are always required when magnetic interfering signals should be remarkably reduced, e.g., when a device must be installed in the vicinity of processes which produce magnetic noise or in a noisy environment of a city. The demands on these shielded rooms vary and depend on the measurement instrument and task. Especially for instruments which are highly sensitive to magnetic fields such as superconducting quantum interference devices (SQUIDs) and electron-beam equipment, the necessity of magnetically shielded rooms is increased. Other applications which require shielding enclosure for the technical frequency range are electron microscopes and large scale exposure equipment in industrial environments, e.g., in semiconductor production and shielding for power transformers when the aim is to shield one particular source of interference. The prime field of application, however, is biomedical diagnostics and research. For example, by using extremely sensitive magnetic field detectors on the basis of SQUIDs, electrical currents of the brain or the heart can be detected via their magnetic field. These magnetic field detectors are very sensitive to the smallest interference fields both in the lower and higher frequency ranges and therefore require shielding enclosure or shielded rooms. At present for such biomagnetic applications, approximately 200 magnetically shielded rooms are installed worldwide. The recorded amplitudes of biomagnetic signals are very weak and range from some femtoteslas for the spinal cord to about 100 pT for the magnetocardiogram (MCG) recorded outside the body, with frequencies from near dc to about 1 kHz. Environmental magnetic noise easily reaches amplitudes of microteslas on top of the static earth magnetic field of about 40 μT. To reduce these magnetic field disturbances magnetically shielded rooms were invented. The eddy-current noise level of the conducting walls should be beneath the noise level of the detector. A very low residual magnetic field and field gradient level inside the room is a further prerequisite for low noise biomagnetic recordings. The residual magnetic field and gradient are determined by the spatial distribution of the residual magnetization along the walls. In combination with mechanical vibration, magnetic field gradients lead to increased noise in the range from 2 to 40 Hz, where most MCG and magnetoencephalograpy (MEG) signals have their main signal power (see Fig. 1). Inside the BMSR-2 we observed a vibration amplitude of about 5 μm for the SQUID sensor system in all spatial directions. Figure 1 demonstrates the noise induced by the mechanical vibration if the magnitude of the field gradient is in the order of 1 pT/mm. By using well balanced gradiometers[1] most of these disturbances will be canceled out. In some applications, however, it is favorable to use magnetometers. Examples for such very sensitive magnetometer recordings which require a very low residual magnetic field and field gradient are the investigation of dc phenomena such as the direct DC-MEG,[2] low-field nuclear magnetic resonance (NMR),[3] and magnetic marker monitoring (MMM).[4] The infrastructure at PTB Berlin provides the framework for such magnetically highly sensitive applications. The new eight-layered magnetically shielded room BMSR-2 of PTB Berlin,[5,6] offers a very high passive shielding factor S, which is 7.5×10^5 at 0.01 Hz and exceeds 1×10^8 above 6 Hz. With additional active shielding S reaches values of more than 7×10^6 down to 0.01 Hz (near dc). In a volume of 1 m^3, inside the room in which most measurements are taken the eddy-current noise level produced by the Permalloy (Mu metal) walls is less than 2 fT/$\sqrt{}$Hz. In the BMSR-2, we run a 304 SQUID vector magnetometer system with a white noise level of less than 2 fT/$\sqrt{}$Hz.[7,8] This instrument represents a reference system for biomagnetic applications. The magnetic field is a vector with three independent components. The gradient of the magnetic field is much more complex. It is a tensor of second order with nine components. Five of them are independent. Nonetheless, with regard to predictions about the reproducibility it is always true that if the residual field is

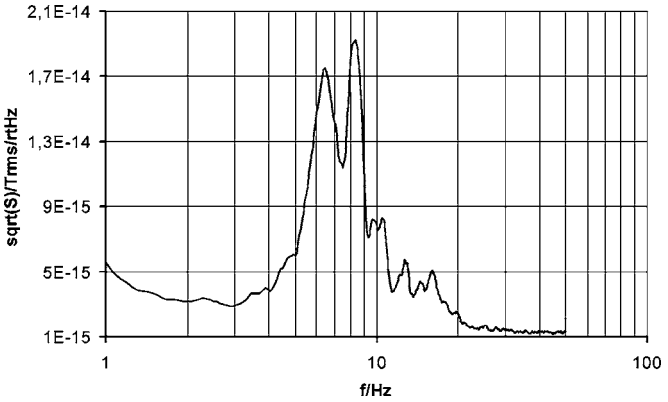

FIG. 1. Flux density noise measured inside the BMSR-2 without any test sample. One of the 304 SQUIDs (Refs. 8 and 25) measuring the vertical field component is depicted. The increased noise level around 8 Hz is caused by mechanical vibrations and the magnetic field gradient of the residual field inside the chamber. The strong noise increase below 1 Hz is due to the $1/f$ noise of the measuring system.

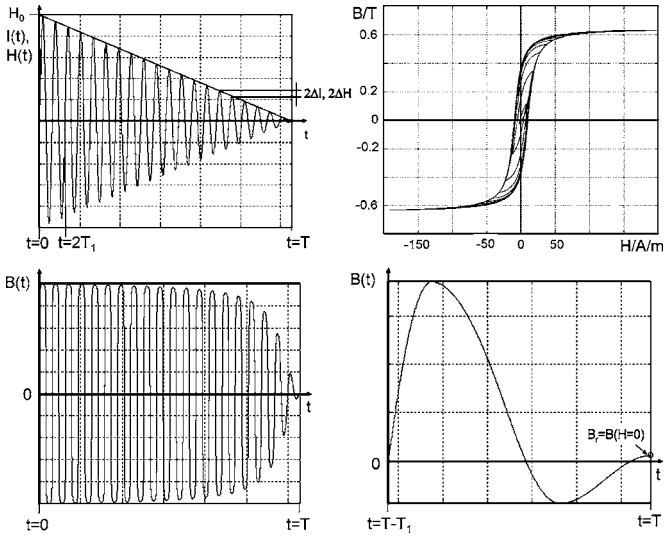

FIG. 2. Upper left: Linearly damped sinusoidal demagnetization function. $N=20$ oscillations. Upper right: Hysteretic $B(H)$ curve. Lower left: Resulting $B(t)$. Lower right: Residual field $B_r=B(H=0)$ at the end of the demagnetization process $t=T$. $B(H)$=Hysteretic model adaptation for Permalloy using the following values: saturation field $B_s=0.63$ T (static), maximum residual field $B_r=0.35$ T, coercive force $H_c=10$ A/m, $f=10$ Hz, 20 periods, and $\Delta H/H_0=2.5\%$.

reproducible the gradient is reproducible, too. For further investigations we therefore always use the residual field instead of the gradient because of its ease of measurement.

Due to the high permeability and the nonvanishing remanence of Mu metal the inner layer (shell) of the shielded room can easily be magnetized by deposing technical magnetic field sources inside the room. We observed a shift of the residual field of up to 30 nT due to regular service works in the BMSR-2. To guarantee low magnetic noise and comparable measurement conditions for the above-mentioned applications the BMSR-2 has to be reproducibly demagnetized. To eliminate accidentally created local magnetizations it is necessary to demagnetize before every measurement session. This procedure preserves our low residual magnetic field of $|\boldsymbol{B}_r|<2$ nT in the measurement volume of 1 m^3. This article deals with the process of demagnetization and the question how to optimize its parameters to reach a reproducible low residual field and gradient inside a magnetically shielded room, which would reduce the flux density noise around 10 Hz (see Fig. 1).

II. THE DEMAGNETIZATION PROCESS

The aim of demagnetization is to reduce the residual magnetic field to the ideal value of $\boldsymbol{B}_i(H=0)=0$ by random orientation of the magnetic domains, in the ideal case in every spatial direction. In practice this is obtained by the application of an alternating magnetic field $h(t)$, e.g., sinusoidal, generated by a current through a coil. The current amplitude decreases depending on the chosen envelope function $e(t)$, e.g., a linear function, starting from a current that yields magnetic saturation inside the ferromagnetic material, down to zero (Fig. 2, upper left sketch). This decreasing alternating magnetic H field forces the magnetization ($M=B-\mu_0 H$) on a cyclic passage through the hysteretic loops from saturation $[B(H_0)]$ into the demagnetized state which is a local state of minimum energy (Fig. 2, upper right sketch). In the case of demagnetization with static fixed coils, an ideal random orientation of the magnetic domains is only obtained in the direction of the magnetic field created by the coil current. Since all magnetic domains were orientated in one spatial direction there should be no magnetization in the two other directions. We applied an envelope function which linearly decreases by ΔH per half period of the excitation signal and reaches $H(t)=0$ at the time $t=T$ (see Fig. 2, upper left sketch).

$$H(t) = \begin{cases} h(t)e(t) = H_0 \sin(\omega t)\left(-\frac{1}{T}t+1\right), & 0 \leqslant t \leqslant T \\ 0, & t<0 \wedge t>T, \end{cases}$$

$$\omega = \frac{2\pi}{T_1}, \quad T = NT_1 \tag{1}$$

where N is the number of oscillations (periods with duration T_1) during the total time duration T of the demagnetization process. Using a current source, the generated field $H(t)$ is related to the applied current $I(t)$ by

$$H(t) = C_G I(t). \tag{2}$$

So, ΔH can also be expressed by ΔI where C_G is a constant geometric factor:

$$\Delta H = C_G \Delta I. \tag{3}$$

The most important figure of the demagnetization function is the progression of the amplitude values in time. The progression of the amplitude values H_i of $H(t)$ [Eq. (1)] is given by Eq. (4), neglecting the time shift of the amplitude position to earlier times when $H \to 0$. This means that Eq. (4) is always true for a large number of oscillations (periods) N in the time interval $(0,\ldots,T)$:

$$H_i = \left| H\left[\frac{T_1}{2}\left(\frac{1}{2}+i\right)\right]\right| = H_0\left[1-\frac{1}{2N}\left(\frac{1}{2}+i\right)\right],$$
$$i=0,\ldots,(2N-1), \tag{4}$$

thus,

$$\Delta H = H_i - H_{i+1} = \frac{H_0}{2N}, \tag{5}$$

and therefore

$$H_i = H_0 - \Delta H\left(\frac{1}{2}+i\right). \tag{6}$$

The amplitudes of the first and last half wave are

$$H_{i=0} = H_0 - \frac{H_0}{4N} = H_0 - \frac{1}{2}\Delta H, \tag{7}$$

$$H_{i=(2N-1)} = H_0\left(1-\frac{1}{4N}-\frac{2N}{2N}+\frac{1}{2N}\right) = \frac{H_0}{4N} = \frac{\Delta H}{2}. \tag{8}$$

In the case of a general envelope function $e(t)$, with a large number of oscillations $(N\to\infty)$, $\Delta H(t_i)/\Delta t$ is equivalent to the first derivative of the envelope function $e(t)$ at $t=t_i$:

$$\Delta H(t) \approx \frac{d}{dt}e(t)\frac{T}{2N}. \tag{9}$$

A. Dependency of the residual field on the step size ΔH

Due to the hysteretic behavior of real ferromagnetic materials, the chosen step size ΔH defines the residual remanence B_r at the end of the demagnetization process when $H(t=T)=0$ [see Fig. 2 lower right sketch and Eq. (8)]. To investigate the dependency of B_r from the step size ΔH we used an algebraic model proposed by de Almeida *et al.*[9] to describe magnetic hysteresis. We adjust this static model to analyze Permalloy (Mu metal). This can be done by adjusting the four parameter model in the same way as shown for a MnZn power ferrite by de Almeida *et al.* The adapted model together with our linear damped demagnetization function with 20 oscillations, i.e., $\Delta H/H_0=2.5\%$ [Eq. (5)], results in the hysteretic loops depicted in Fig. 2. The field $B(t)$ resulting from our adapted model after applying the demagnetization function using 20 oscillations $(\Delta H/H_0=2.5\%)$ is depicted in Fig. 2 (lower left sketch). To clarify exemplarily the deviation of the residual magnetic field $B_r=B[H(t=T)]=0$ from the ideal value $B_{ir}=0$ at the end of the demagnetization process the last period of $B(t)$ is extracted in Fig. 2 (lower right sketch).

As a rule of thumb, in Ref. 10 it is recommended that ΔH should be chosen less than 1%–2% of the coercive force H_c. Using the model values for $H_c=10$ A/m and $H_0=150$ A/m for the H field necessary to reach the saturation field strength H_s Eq. (5) delivers a number of periods $N=750$ for $\Delta H/H_c=1\%$. In Fig. 3 the absolute value of the residual field normalized to the saturation field strength $B_s=0.63$ T with increasing ΔH is shown. We called the normalized deviation E_B for "Error" of field B since this value should be zero for a perfect demagnetization.

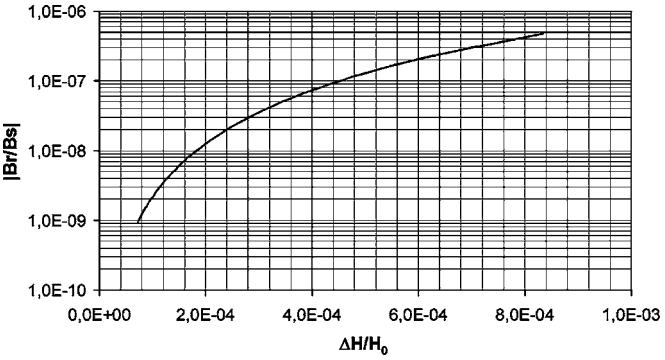

FIG. 3. Error $E_B=|B_r/B_s|$ of B for $H(t=\mathrm{T})=0$, dependent on $\Delta H/H_0$.

$$E_B = \left|\frac{B_r}{B_s}\right|. \tag{10}$$

Figure 3 displays the progression of E_B with increasing ΔH. This dependence of E_B from ΔH can be approximated for $\Delta H/H_0<0.08\%$, i.e., $N>600$ by the following fitting function:

$$E_B = \left|\frac{B_r}{B_s}\right| = \gamma\left(\frac{\Delta H}{H_0}\right)^{\beta} = \gamma\left(\frac{1}{2N}\right)^{\beta} \quad \text{for } N>600. \tag{11}$$

where

$$\gamma=\alpha(100)^{\beta-1}=31.8, \alpha=0.0261, \quad \text{and } \beta=2.54.$$

The fitting function in Eq. (11) can be reversed so that it is possible to estimate the necessary step size ΔH to achieve a given magnetic field limit.

$$\frac{\Delta H}{H_0} = \left(\frac{E_B}{\gamma}\right)^{1/\beta} = \left(\frac{1}{\gamma}\left|\frac{B_r}{B_s}\right|\right)^{1/\beta} \quad \text{for } N>600. \tag{12}$$

The adapted model of de Almeida *et al.* is only valid for a homogeneous closed loop structure like a toroid of ferromagnetic material. Although each of the seven shells of the BMSR-2 forms a closed loop, its structure is far from homogeneous and therefore the application of this model is a simplification. Each magnetic shell consists of a complex arrangement of plane and edge elements built up with strips of 0.5 mm thick annealed Mu-metal sheets also used for the conventional shielded rooms. This arrangement of strips is a noncontinuous closed loop structure with many slots. A slot in the pathway of the magnetic flux guided by a ferromagnetic structure leads to shearing of the hysteretic $B(H)$ curve and therefore to a flattening of the hysteretic loops. A sheared hysteretic curve gives smaller residual fields at the end of the demagnetization process. Thus, the residual field produced in the BMSR-2 is smaller than the values given by our adapted model. Though a sheared curve gives lower values of the residual field, it is at the expense of a saturation state which is reached at much higher-field strengths.

B. Interrelations between residual field, reproducibility, and step size ΔH

In general the fact that repetitive applications of a similar demagnetization process, such as that described above, lead to a number of scattered values around a certain value of the residual field B_r (Ref. 11) indicates that each B_r is a

realization of a stochastic process. The following provides an explanation of the underlying physical processes. We will see later in Sec. III E that the demagnetization hardware adds additional contributions to this stochastic process.

The variance, the absence of reproducibility, is a natural result of the combination of environmental noise, including thermal effects, and the dynamic complexity of systems with many interacting degrees of freedom. At $T=0$ K, reproducibility is always achieved.[12] In ferromagnetic materials, the effective field acting on each spin magnetic dipole is the vector sum of the applied field plus a strong interacting field arising from all the neighboring dipoles. This internal field can be expressed by

$$B_{\text{in}} = \mu_0(H_{\text{in}} + \alpha M), \tag{13}$$

where α is a mean field parameter representing interdomain coupling, which may be determined experimentally.[13] Consider the energy E per unit volume of a typical domain with magnetic moment per unit volume m in a magnetic field H_{in}:

$$E = -\mu_0 m H_{\text{in}}. \tag{14}$$

Inside a ferromagnetic solid there will be coupling between the domains and consequently, if this is expressed as a coupling to the bulk magnetization M,

$$E = -\mu_0 m(H_{\text{in}} + \alpha M). \tag{15}$$

In the case of $\alpha \neq 0$ this approach leads to the modified Langevin equation for bulk magnetization[13] of an ideal ferromagnetic crystal:

$$\frac{M}{M_S} = \coth\left[\frac{\mu_0 m(H_{\text{in}} + \alpha M)}{k_B T}\right] - \frac{k_B T}{\mu_0(H_{\text{in}} + \alpha M)}. \tag{16}$$

There M_S is the saturation magnetization.

Assuming no field H_{in}, which is the case at the end of the demagnetization process, the energy per unit volume is exclusively determined by the bulk magnetization due to interdomain coupling and can be expressed by the internal field B_{in} at $H=0$:

$$E = -\mu_0 m \alpha M. \tag{17}$$

Each remaining, i.e., induced, local magnetization M in the material leads to a proportionate (α) energy increase (alignment of spin moments) of the domains. Such a magnetization can be easily formed in real ferromagnetic structures.

In an ideal ferromagnetic crystal at $T=0$ K forming a macroscopic specimen, each value of the $B(H)$ diagram is identical with the anhysteretic curve. Demagnetizing such an ideal crystal with an ideal demagnetization function ($\Delta H \rightarrow 0$) always reaches the state of minimized energy (paramagnetic state) where the ideal residual field $B_i(H=0)=0$ is reached. The propagation of $B(H)$ is deterministic (reproducible), follows the anhysteretic curve, and can be described by the Langevin equation for bulk magnetization.[13] This is the lossless case, no energy remains stored in the system at $H=0$. A real ferromagnetic crystal at $T=300$ K (thermal noise) exhibits a lack of uniformity caused, e.g., by impurities (e.g., magnetic or nonmagnetic inclusions) or local stress, which form pinning sites creating metastable states for the Bloch walls. These pinning sites shape a complex energy landscape. The motion of the domain walls through this energy landscape under the influence of an applied magnetic field is impeded by the presence of this lack of uniformity in the lattice. The flexible Bloch walls are distorted or pinned which is equivalent to the storage of energy in the system due to the corresponding local magnetization.[14] Thus, certain energy is needed to overcome such metastable states. This is the cause of the hysteretic behavior of real ferromagnetic structures and the residual field at $H=0$.[15,16]

The number of possible metastable states of a macroscopic nonideal sample is enormous; each repetition of the magnetization/demagnetization process follows a different trajectory among the energy landscape.[17,18] An arbitrarily small amount of noise, coupled with the wall dynamics, will allow the system to sample all possible routes through the disorders. This variability is a measure of the distribution of possible paths of the domain wall.[12] Therefore, each path is a realization of a stochastic process. Thus the residual field B_r for each zero crossing of the excitation field H is a stochastic variable with the mean value $\mu(B_r)$ and a standard deviation $\sigma(B_r)$ assuming a Gaussian distribution. At the end of the demagnetization process $\sigma(B_r)$ is equivalent to the reproducibility of the remaining residual field. Applying an ideal demagnetization function on a real sample, the probability of overcoming the pinning sides is high. Therefore the energy minimum of this system is reachable. The Bloch wall movement is not affected by pinning but is distorted. The amount of energy which remains in the system leads to an energy level at the end of the demagnetization process $[B(H=0)]$ which is different from that in the ideal case. Therefore, a residual field B_{ir} with mean value $\mu(B_{ir})$ and the standard deviation $\sigma(B_{ir})$ beyond $B_i=0$ is reached. The only method which reaches the ideal demagnetized (paramagnetic) state is heating (annealing) of the ferromagnetic structure beyond the Curie temperature (380 °C for Mu metal) where a ferromagnetic specimen becomes paramagnetic. It then has to be cooled down inside a zero magnetic field. This method is unfortunately inappropriate for our application.

The application of a nonideal demagnetization function, i.e., ΔH has a finite value far above the thermal noise, increases the probability of pinning, which means that magnetization occurs at that pinning site. In that case, more energy is stored. This leads to a higher energy level at $H=0$ and therefore to a higher residual field B_{rr} $[\mu(B_{rr}), \sigma(B_{rr})]$ at the end of the demagnetization process.

The increased tendency of pinning also leads to new realizations of the stochastic process (additional subpaths) which broadens the distribution function of the stochastic variable B_r and means that $\sigma(B_r)$ increases.[18,19] The increase of $\sigma(B_r)$ with increasing ΔH was shown experimentally by Ref. 20. We will also experimentally prove the validity of this effect on our shielded room in Sec. V A.

To summarize, a demagnetization process with a large decrease in the supplied energy from halve wave to halve wave (large ΔH) leaves Bloch walls trapped or bent at certain metastable states (pinning sites). This is equivalent to a local magnetization which influences the domains in the vicinity of this magnetization. Therefore energy remains stored in the system which leads to an increase in the residual field $\mu(B_r)$ and to a worsening of reproducibility $\sigma(B_r)$.

C. Criteria for low residual field demagnetization

Every half wave of the demagnetization signal provides the energy to force the magnetic domains, i.e., the Bloch walls, in one direction leaving an amount of magnetic moments behind which were aligned by the energy of the former half wave in the opposite direction.

In the linear decreasing case, an ideal random spatial orientation of the magnetic domains is achieved by an infinite number of periods in T, which also means $\Delta H \rightarrow 0$. This is equivalent to a negligible energy reduction from halve wave to halve wave and therefore the amount of left-behind spins is small. This ensures that the spatial distribution of domains is such that the net magnetization tends towards zero. A descriptive explanation is that the variation of ΔH leads to a fragmentation of the demagnetized structure, coarser or finer, dependent on ΔH (simplified model: checkerboard pattern). Assigning this explanation to our Mu-metal shell gives a good idea of the increase of the residual field gradient assuming a coarse fragmentation corresponding to a large ΔH. In the extreme case of a demagnetization function utilizing only one period the ferromagnetic shell of the magnetically shielded room is fragmentized into large areas. Inside the shell, the large magnetic areas create a strong magnetic field gradient.

We searched for a figure of merit which enables a prediction about the result of the demagnetization process which does not necessarily include the exact contributions of the ferromagnetic material (i.e., B, μ_r) which is hard to measure exactly for every part of a complex geometrical structure such as a magnetically shielded room. Furthermore this figure should deliver a set of available parameters which are elements of the excitation signal H and whose variation significantly affects the outcome of the demagnetization process.

Every halve wave of the excitation field H forms a corresponding area in the $B(H)$ diagram whose size depends on the applied envelope function. This area is enclosed by the hysteretic curve in the corresponding quadrants (1 and 4, or 2 and 3, see Fig. 2) dependent on the polarity of the excitation halve wave. This area is a measure for the energy per unit volume which must be provided by the current source. During demagnetization, the $B(H)$ area (energy per unit volume) created by one halve wave of $H(t)$ differs by a certain amount in comparison with the area formed by the previous halve wave. The energy per unit volume E provided by a halve wave of the sinusoidal excitation field H follows Warburg's law:

$$E = \int_{B(t_1)}^{B(t_2)} H(t)dB = \int_{B[(T_1/2)i]}^{B[(T_1/2)(i+1)]} H(t)dB = \int_{(T_1/2)i}^{(T_1/2)(i+1)} H(t)\frac{dB}{dt}dt. \tag{18}$$

We define a parameter D,

$$D = \int_{t_1}^{t_2} H(t)dt = \int_{t_1}^{t_2} e(t)h(t)dt, \tag{19}$$

which is the difference of the positive and negative areas of two consecutive half waves of the demagnetization function in a regarded time range. If $h(t)$ is a sinusoidal function, the parameter D can also be rewritten in the following way:

$$D = \left[-\frac{H_0 e(t)}{\omega} \cos(\omega t) \right]_{t_1}^{t_2} + \frac{H_0}{\omega} \int_{t_1}^{t_2} \frac{de(t)}{dt} \cos(\omega t)dt. \tag{20}$$

With the boundaries $t_1=0$ and $t_2=T$, $e(t)$ must be

$$e(t_1 = 0) = 1 \quad \text{and } e(t_2 = T) = 0.$$

Thus follows for D,

$$D = \frac{H_0}{\omega}\left[1 + \int_0^T \frac{de(t)}{dt} \cos(\omega t)dt \right] = \frac{H_0}{\omega}\left[1 + \frac{2N}{T}\int_0^T \Delta H(t)\cos(\omega t)dt \right]. \tag{21}$$

In this case D is the mean imbalance between the positive and negative excitation areas in the time range from $(0,\ldots,T)$. If $\Delta H(t)$ is a constant value ΔH, i.e., $e(t)$ is a linear function with N oscillations in T, the integral in Eq. (21) vanishes and D results in

$$D_{\text{lin}} = \frac{H_0}{\omega}. \tag{22}$$

Although D is a very insensible parameter it can help us to classify possible demagnetization functions because it does not need any information about the ferromagnetic structure or the resulting $B(t)$. In the following we will provide evidence for the prediction that a decreased D correlates with a smaller residual field. A more sensible expression of the imbalance of the magnetic moment alignment is given by the change of energy between two consecutive halve waves of $H(t)$. If N is large, the energy change is given by [using Eq. (18)]

$$\frac{dE}{dt} = H(t)\frac{dB[H(t)]}{dt} = \frac{dD}{dt}\frac{dB}{dt} = H(t)\frac{dH(t)}{dt}\frac{dB}{dH} = H(t)\frac{dH(t)}{dt}\mu_r(H)\mu_0 = \frac{d}{dt}\left[\frac{H^2(t)}{2}\right]\mu_r(H)\mu_0. \tag{23}$$

The energy change is shaped via the interplay of $H(t)$ and the material characteristics $\mu_r(H)$. Our proposal is to use the material characteristics dB/dH to create an adapted demagnetization function. This can be accomplished in the following way. Using a linear decreasing demagnetization function $H(t)$ on a ferromagnetic structure, starting from saturation, B is forced via $H(t)$ on a cyclic passage through the minor hysteretic loops. The tips $(B_{\max}, H_{\max})$ of the minor loops lie on the initial magnetization curve (commutation curve and anhysteretic curve) (see Fig. 2, upper right sketch and Fig. 4 right sketch). Measuring the flux density $B(t)$ with a search coil, the envelope of $B(t)$ is a good approximation of the form of the materials' reversely traversed initial curve (see

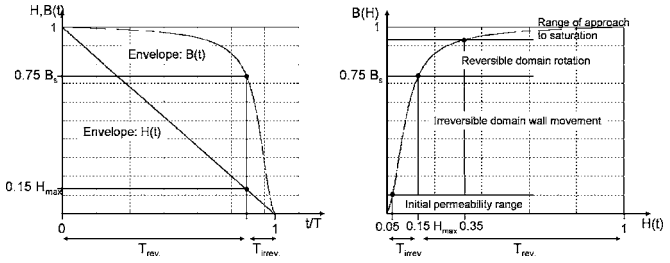

FIG. 4. Normalized envelopes of $H(t)$ and $B(t)$ and the normalized initial magnetization curve obtained from modeled Permalloy. The values T_{irrev} and T_{rev} mark the time/H-field intervals where irreversible, or reversible, domain processes dominate.

Fig. 2, lower left sketch and Fig. 4 left sketch). Normalizing and time reversing lead to the initial $B[H(t)]$ curve depicted in Fig. 4 on the right side.

Passing through the different parts of the initial magnetization curve (Fig. 4 right sketch) reversible and irreversible domain processes arise. The part for very low fields is called the Rayleigh region where reversible domain boundary displacements take place. The steepest part, where $\mu_r\mu_0 = dB/dH$ becomes maximal, is called the region of irreversible domain boundary displacements or irreversible magnetization. With further increase in the H field follows the reversible transition into the range of approach to saturation via a process called domain rotation. Both are reversible processes.[16] Irreversible processes are caused by a lack of uniformity in the specimen. This lack is determined by many factors, among the most important of which the following may be listed: gross composition, impurities, fabrication, heat treatment, temperature, and stress.[14,15]

In the steepest part of the anhysteretic curve, irreversible processes dominate. Based on our conclusions given in the previous section we recommend a small energy step size (dE/dt should be small) in this region to increase the probability of overcoming the energy barriers formed by these pinning sites. A demagnetization process with a large decrease in the supplied energy from halve wave to halve wave leaves Bloch walls trapped or bent at this pinning center. An amount of magnetization is left behind which increases the residual field. In contrast to this, the region of reversible processes can be traversed with very large dE/dt because the parallel alignment of the magnetic moments in this range is an elastic process. The energy to turn the moments back into their easy axis is provided by the influence of the lattice or inner stress. The distribution of demagnetization energy over the different regions, i.e., the demagnetization time intervals, can be determined by the shape of the envelope function $e(t)$. The number of oscillations in a certain part of the initial curve is proportional to the residence time $(T_{\mathrm{rev}}, T_{\mathrm{irrev}})$ of the demagnetization process in that region (see Figs. 2 and 4). A large ratio of $T_{\mathrm{rev}}/T_{\mathrm{irrev}}$, i.e., a small T_{irrev}, is an indicator of a small energy change in the region of reversible processes. The demagnetization factor K of a ferromagnetic structure at the local measurement position of $B(t)$ introduces a shearing into the measured initial curve in the following way:

$$\underline{B}_{\mathrm{eff}} = \underline{B}_0 - \underline{\mu}\underline{\underline{K}}\underline{M}. \tag{24}$$

Although it is difficult to estimate the demagnetization tensor $\underline{\underline{K}}$ for a complex ferromagnetic structure, the ratio of the

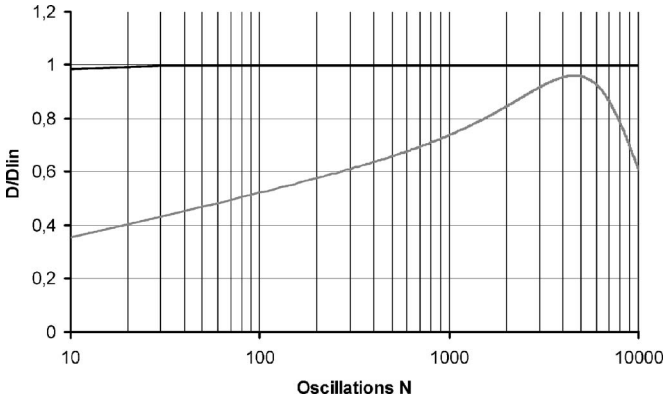

FIG. 5. D/D_{lin} in the time range $(0,\ldots,T)$, with increasing N for the exponential (black line) and logarithmic (gray line) decreasing envelopes for $e(t)$. $a=8$ for the exponential case. With $a=0.0921$, $b=-5.9572$, $c=6.1553\times10^{-5}$, and $d=-0.1474$.

$T_{\mathrm{rev}}/T_{\mathrm{irrev}}$ (see Fig. 4) is not affected by the shearing process. T_{irrev} marks the interval where the region of irreversible domain processes dominates. In Fig. 4, this is the range where H falls below $0.15H_{\max}$ ($\approx$10 A/m) and B falls below $0.75\,B_s$ ($\approx$0.48 T). We do not further distinguish between the time interval of the irreversible processes and the Rayleigh region. The inclusion of the initial permeability range into time interval T_{irrev} is possible because of the predominance of reversible domain processes and of its relative smallness.

To test our predictions we applied two additional envelope functions on our modeled demagnetization process and compared them with the results given by the linear decreasing $e(t)$. The first envelope function is an exponentially decreasing $e(t)$ of the following form:

$$e_{\mathrm{expt}}(t) = e^{-\alpha(t/T)}, \quad \alpha > 1. \tag{25}$$

With $T=2\pi N/\omega$, D for this $e(t)$ becomes

$$D_e = \frac{H_0}{\omega}\left\{\left[\left(\frac{\alpha}{2\pi N}\right)^2 + 1\right]^{-1}(1-e^{-\alpha})\right\} \times \overset{(\alpha/2\pi N)\to 0}{\longrightarrow} \frac{H_0}{\omega}(1-e^{-\alpha}). \tag{26}$$

With the requirement that $\alpha>1$, it is shown that D can be lowered in comparison with the linear decreasing case for $e(t)$. The second function was especially designed to meet the above-mentioned criteria and is logarithmic shaped

$$e_{\log}(t) = a\,\ln\left[\frac{T(b-c)+t}{cT-t}\right] + d, \tag{27}$$

where a, b, c, and d are constant values.

$$D_{\log} = H_0\int_0^T e_{\log}(t)\sin(\omega t)dt. \tag{28}$$

The solution of $D_{\log}$ is a cumbersome expression incorporating the sine integral and cosine integral which hinders a fully analytical solution. Therefore a numerical calculation of $D_{\ln}$ was carried out. The propagation of D_e/D_{lin} and $D_{\ln}/D_{\mathrm{lin}}$ is depicted in Fig. 5. Without further analysis of the shape of $D_{\log}/D_{\mathrm{lin}}$ it is true to say that $D_{\log}$ is always smaller than D_e

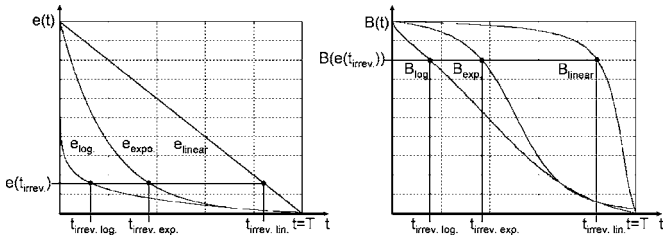

FIG. 6. Envelope function $e(t)$ of the excitation field $H(t)$ (left sketch) and the envelope function of the resulting $B(t)$ (right sketch) for a linear, exponential, and logarithmic decreasing excitation field $H(t)$. The time T_{irrev} is marked, after that the individual envelope function places demagnetization cycles in the section of the demagnetization process where irreversible domain processes dominate.

and D_{lin}. Figure 6 displays the variation of the envelope of $B(t)$ and the decrease of t_{irrev}, which marks the entry into the region of irreversible processes, with the application of the three different envelopes $e(t)$ for $H(t)$.

Considering only the envelope $e(t)$ we calculated the first derivate of the energy for the three applied envelope functions (Fig. 7). This gives an impression of the variation of energy in certain time intervals.

Figure 7 nicely depicts how the different functions modulate dE/dt after the region of irreversible processes is reached at $t=t_{\text{irrev}}$. Applying D to Eq. (18) leads to

$$E = \left(D\frac{dB}{dt}\right)_{t_1}^{t_2} - \int_{t_1}^{t_2} D\frac{d^2B}{dt^2}dt. \tag{29}$$

If the traversing of the region of irreversible processes comes along with a linear decreasing $B(t)$ in this range, which is approximately the case when applying a logarithmic envelope, Eq. (25) reduces to the following expression:

$$E_{\text{irrev}} = (D\ \text{const})_{t_{\text{irrev}}}^{T}, \qquad \frac{dE_{\text{irrev}}}{dt} = \left(\frac{dD}{dt}\text{const}\right)_{t_{\text{irrev}}}^{T}. \tag{30}$$

For further investigations we will only consider the comparison between the logarithmic and the linear functions. To verify a possible improvement in the residual field by applying a demagnetization function with the above-mentioned characteristics [small D in $(0,\ldots,T)$, dE/dt large in $(0,\ldots,T_{\text{rev}})$, dE/dt small in $(0,\ldots,T_{\text{irrev}})$] we calculated the residual field after demagnetization for $t=T$ applying the envelope $e_{\text{lin}}(t)$ and $e_{\log}(t)$ for increasing numbers of oscillations N in the same way as was done in Sec. II A. Figure 8 displays the comparison of the decrease in the relative residual field $|B_r/B_s|$ for a certain N by using the logarithmic decreasing envelope function and the linear decreasing function. The calculation shows that by applying the logarithmic envelope a lower residual field is gained in comparison with the linear decreasing envelope with the same amount of cycles.

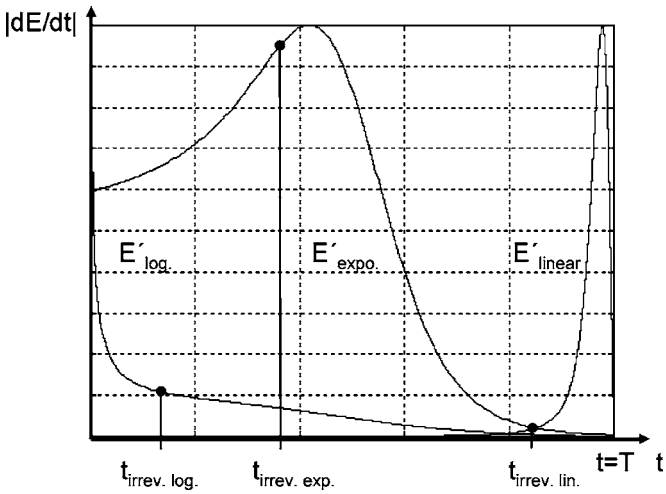

FIG. 7. Normalized absolute values of the time slope of the energy change for a linear, exponential, and logarithmic decreasing envelope for the excitation field $H(t)$.

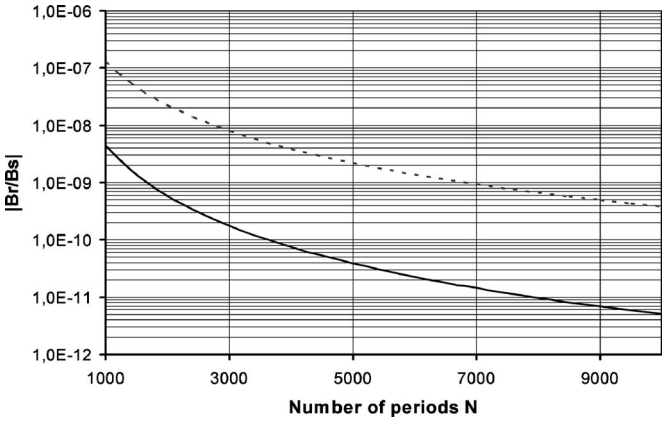

FIG. 8. $|B_r/B_s|$ at $t=T$ for different N. Dotted line: $|B_r/B_s|(N)$ in the linear decreasing case. Black line: $|B_r/B_s|(N)$ in the logarithmic decreasing case.

We verified our findings by experiment on a closed Mu-metal disk of 180 mm diameter and 0.5 mm thickness (provided from VAC, Germany). We placed the disk inside the BMSR-2 and applied the linear and logarithmic $e(t)$. The residual field after the demagnetization was measured 15 mm above the disk plane with a spatial resolution of 15 mm using a three-axis fluxgate (Bartington 03MC-L7) with a resolution of about 1 nT.

After applying a linear $e(t)$ with $N=1000$, the residual field was close to the resolution boundary of the fluxgate sensor. Then we applied the linear $e(t)$ with $N=50$ which led to a peak value of the field component perpendicular to the disk of around $|B_z|=20$ nT and a coarse distribution of local magnetization, means a large field gradient (Fig. 9, left

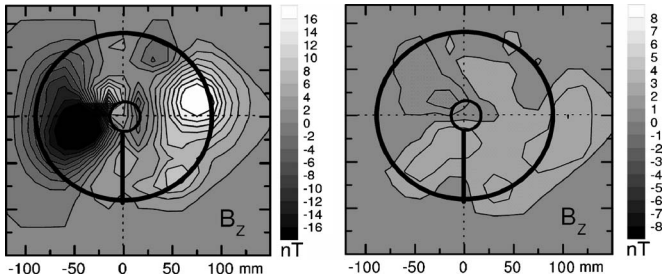

FIG. 9. B_z component 15 mm above a Mu-metal disk (180 mm diameter). Left: B_z after applying a linear decreasing envelope function with $N=50$. Right: B_z after applying a logarithmic decreasing envelope function with $N=50$. The silhouette of the Mu-metal disk is highlighted by the bold black circles. The position of the excitation coil is highlighted by the vertical bold black line.

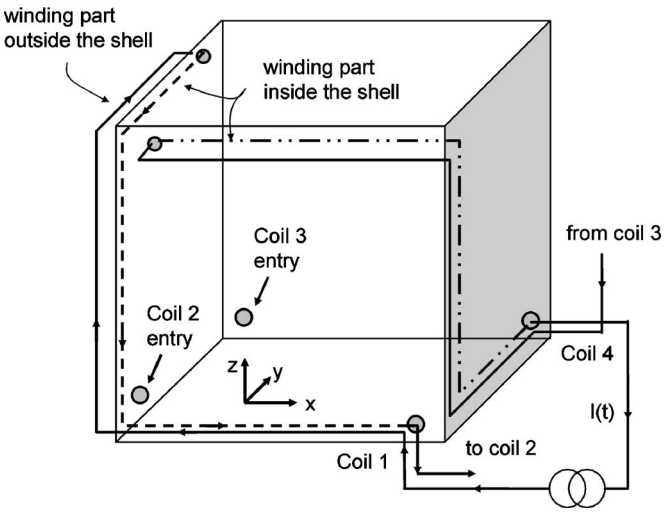

FIG. 10. Coil arrangement for one shell of the BMSR-2. Only one of the seven windings is shown for coils 1 and 4. Coils 2 and 3 are omitted for clarity.

sketch). After reapplication of the linear $e(t)$ with $N=1000$ for "erasing" the disk, the logarithmic $e(t)$ with $N=50$ was applied (Fig. 9, right sketch). The residual field in the B_z direction for this function falls in the range of the linear $e(t)$ for $N=1000$ ($|B_z|=2$ nT), with a smooth distribution of local magnetization. This experiment proves that with increasing step size the residual field and field gradient above the surface of this simple ferromagnetic structure are reduced.

From these theoretically, analytically, and experimentally obtained findings we conclude that an improvement of demagnetization can be achieved by fulfillment of the abovementioned criteria: dE/dt large from the beginning up to the entry of the region of irreversible processes and small afterwards which also means a decreased D. According to the explanation given above, a small dE/dt in the irreversible region 2 defines the smoothness, i.e., the grade of fragmentation done by the demagnetization process on the ferromagnetic structure. Thus optimizing the demagnetization process is possible by minimizing dE/dt in this regime. In the following we will call dE/dt the fragmentation parameter.

III. MATERIALS AND METHODS

A. Geometric aspects of the demagnetization coils

The BMSR-2 comprises seven magnetic layers of Mu metal (Vacuumschmelze, Hanau, Germany. Chemical composition: 76.6% Ni; 4.5% Cu; 14.7% Fe; 3.3% Mo; Mn; Si; etc.) with a total weight of 24.3t and one highly conductive eddy-current layer made of 10 mm aluminum. The working space enclosed is $2.9\times2.9\times2.8$ m^3. In order to demagnetize the chamber, each Mu shell has a specific arranged set of four coils (Fig. 10) to generate a magnetic field flowing inside the walls around the x, y, or z axis.[5,6]

Together with the Mu metal, each interconnection of the four coils is a large inductance with an impedance of about $Z_L=2.2\ \Omega+7j$ mH. The diameter of the copper wires used restricts the maximum effective current. We apply an effective current of up to 50 A to demagnetize one shell. The chamber is demagnetized shell by shell.

Each coil starts at one corner of the shell at the bottom of the xy plane and continues along the bottom edge to the corner on the left-hand side. There it turns 90° in the direction of the z axis and further proceeds to the corner at the ceiling (highest xy plane). At the ceiling it again turns 90° and continues along the edge parallel to the ceiling towards the next corner. There it changes from the outside to the inside of the shell. From that point it follows the same way in the reverse direction. Every direction in space of the shell can be demagnetized separately using different interconnections of the four coils. This means that the pathway of the flux circulating through the Mu-metal walls differs by the interconnection used. As shown above, the arrangement of the demagnetization coils for every shell of the BMSR-2 yields to an inhomogeneous field distribution inside the Mu-metal walls, which leads to a spatial field sensitivity of the walls. Parts of the walls near the coils, especially the corners, reach the state of saturation at lower currents than central parts of the wall. Experimentally, we found that a one half wave sinusoidal excitation with an amplitude of at least $I=1$ mA results in a remaining residual field shift in the center of $\Delta|\mathbf{B}_r|=27$ pT. Consequently, small constant or time-dependent currents, such as randomly distributed transient pulses, magnetize the walls close to the coils and also where superimposed fields of different wires reach a local maximum. This leads to a stochastic deviation around the mean value of the residual field measured in the center of the chamber after demagnetization and therefore to a decrease of reproducibility. In the following we call this phenomenon of the chamber current sensitivity. According to Sec. I, to reach a residual field below 1 nT ($E_B=B_r/B_s<0.0016$ ppm) close to the walls, as we would like for the BMSR-2, a step size smaller than $\Delta H/H_0=0.009\%$ [see Eq. (11) and Fig. 3] is required which corresponds to a demagnetization procedure with more than $N=5500$ oscillations. In contrast to this, when applying the rule of thumb ($\Delta H/H_c<1\%-2\%$) proposed in, Ref. 10, we calculate a $\Delta H/H_0$ of 0.06%. This gives us an error of $E_B<0.27$ ppm and yields an inconvenient large residual field B_r near the walls of around 170 nT.

B. Measurement of residual fields below 1 nT

To evaluate the absolute residual field vector $\boldsymbol{B}_r=(B_x,B_y,B_z)$ we measured at fixed points inside the room. A vector magnetometer system, consisting of six integrated multiloop dc SQUIDs in a cubic arrangement, was used.[21] The cube design allows the estimation of all vector components at the center of the cube by averaging the SQUID signals at opposite sides. For a measurement of the static magnetic field the dc offset of the sensor pairs must be known. Generally, the dc offset of a sensor pair can be determined by a rotation of the cube around the cube center. The average of the measured field values in both positions is the dc offset of the pair. To determine the x- and y-dc offsets we simply rotate the whole Dewar 180° around its z axis since the cube is fixed on the z axis of the Dewar. It is not possible to turn our Dewar upside down. The rotation for the z-dc offset is replaced by a tilt of 40° around the x axis and a following 180° rotation around its z axis. Together with the already known x- and y-dc offset the z-axis dc offset can by

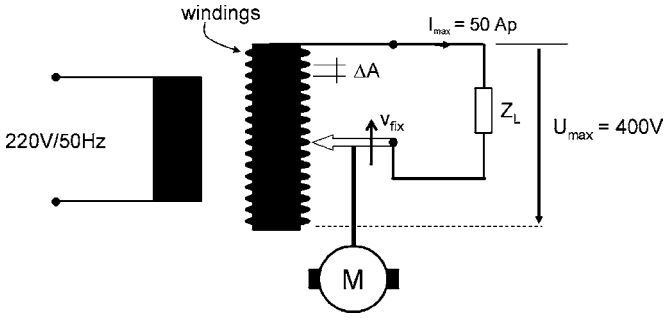

FIG. 11. Motor-driven demagnetization equipment. Secondary windings are highlighted.

calculated. Prerequisite for the calibration and the following measurements is that all SQUIDs remain permanently locked in flux-locked-loop mode. The method offers an absolute magnetic field measurement with an uncertainty of ±20 pT.[22]

C. Typical equipment for demagnetization

Conventional equipment for demagnetizing shielded rooms consists of a variable transformer (variac) which operates directly from mains 220 V/50 Hz(60 Hz). Simple models use a hand wheel to change the voltage. Advanced systems comprise a motor-driven slider contact gliding over the secondary windings (Fig. 11). The number of windings determines $\Delta H(\Delta I)$. The duration T of the demagnetization process is given by the fixed velocity v_{fix} of the motor-driven slider contact. Assuming a linear decreasing envelope for the degaussing function with a fixed step size of more than $\Delta H/H_0 > 0.1\%$, i.e., 1000 secondary windings, the application of Eq. (11) approximates a residual field near the walls of $|\boldsymbol{B}_r| > 480$ nT.

To get a smoother envelope function our variable transformer is equipped with three parallel slider contacts, as depicted in Fig. 12. The movement of the slider contact over the windings generates an envelope function for $I(t)$ similar to that depicted in Fig. 12.

During the passage of the slider contact over the windings the momentary amplitude of the sinusoidal function stays constant as long as the slider keeps contact with the actual winding. The transition to the next winding is characterized by a time interval where two adjacent windings are short-circuited by the slider contacts. This creates an intermediate state between the two levels (see Fig. 12 at $t=t_3$).

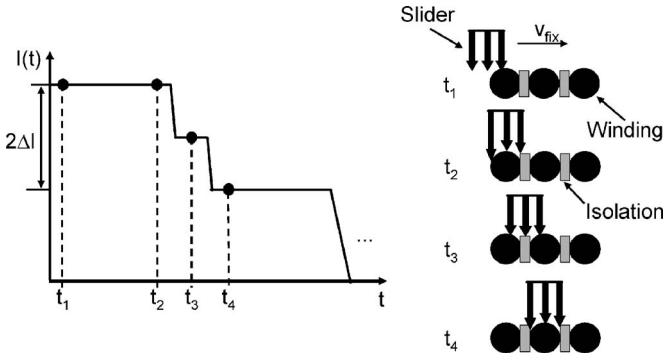

FIG. 12. Part of the envelope function generated by the movement of the slider contacts over the windings.

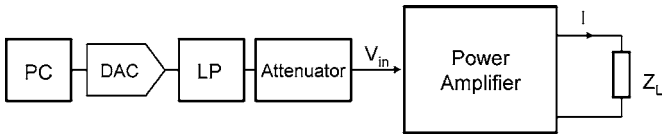

FIG. 13. Basic stage. Z_L, impedance of the degaussing coil of one Mu shell is about $2.2\ \Omega + 7j$ mH. LP, low pass filter. Attenuator (20 dB) to preserve the dynamic range of the DAC.

The load changes in steps. This is a potential source of strong transient pulses. The height of the transient pulse generated at the end of the process when the slider leaves the last winding correlates with the amplitude of the last halve wave. We measured an amplitude of the last half wave of 250 mA with a polarity dependent on the random start polarity. We observed that these transient pulses produced a field shift of about $\Delta|\boldsymbol{B}_r| \approx 220$ pT in the center of the room. Using this equipment on the BMSR-2 a reproducibility of $\sigma(|\boldsymbol{B}_r|) = 300$ pT was measured.

With similar equipment (REO transformer, type RRTEN7, $I=20$ A, $f=50-400$ Hz, 330 windings) we demagnetized a conventional cabin [AK 3b (Ref. 23)] with two Mu-metal layers and one eddy-current layer having similar demagnetization coil arrangement to that installed in the BMSR-2. The shielding factor of the AK 3b reaches values of $S(0.1\ \mathrm{Hz})=100$, $S(0.01\ \mathrm{Hz})=30$, which were measured by. Ref. 24. The duration of the demagnetization process is nearly $T=60$ s which results in a plateau time of the envelope of $T_P=60$ s/330 steps=0.1818 s/step. With a 50 Hz($T=0.02$ s) frequency of the excitation signal, the number of oscillations without change in amplitude becomes $T_P/T=9.09$. Estimating the endpoint error applying Eq. (11) with $\Delta H/H_0 > 0.3\%$, i.e., more than 330 steps, yields $|\mathbf{B}_r| < 8\ \mu$T. Measuring the residual magnetic field using a fluxgate yields $|\boldsymbol{B}_r| \approx 1\ \mu$T near the walls. The value measured includes the fraction of the damped earth's magnetic field of <400 nT, assuming $S=100$. Nonetheless, this measurement is in the order of the theoretically derived value for the residual field $|\boldsymbol{B}_r|$.

D. Improved demagnetization unit

To meet the demands of ΔH mentioned above and to stay below the experimentally gained values for the current sensitivity, we followed a different approach compared to the typical one, which allows the application of smaller values ΔH and a selectable demagnetization function. A gradient power amplifier (Bruker B-GS 350) usually used for magnetic resonance imaging (MRI) was installed. The output current is controlled by a free programmable demagnetization function generator consisting of a Personal computer (PC) with a digital to analog converter (DAC) (Fig. 13). The high current needed ($I_{\mathrm{rms}}=50$ A) and the ability to drive large inductive loads (>7 mH per shell) without oscillations prohibit the application of a conventional four-quadrant power supply.

Like every high power amplifier it suffers from offsets, drift, and transient pulses. Additional perturbation signals occur from the interconnection between the different instru-

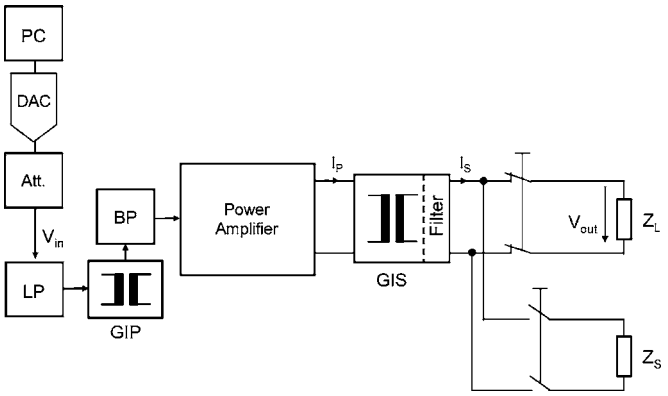

FIG. 14. Further improved demagnetization unit. Z_L, impedance of the degaussing coil of one Mu shell is about 2.2 $\Omega+7j$ mH. Z_S, substitute load. LP, reconstruction low pass filter. BP, bandpass filter. GIP, galvanic isolation primary side. GIS, galvanic isolation secondary side. 20 dB attenuator (Att.) to preserve the dynamic range of the DAC.

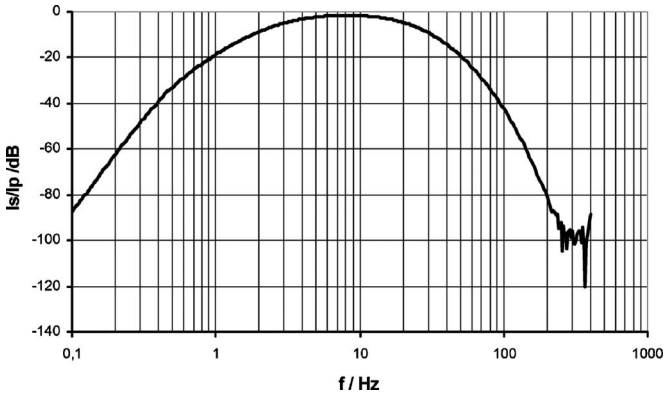

FIG. 15. Transfer characteristic of the whole signal chain centered at 10 Hz. I_S, current of the secondary side. I_P, current of the primary side.

ments. The reproducibility $\sigma(|\boldsymbol{B}_r|)$ was still similar as with the conventional equipment.

E. Reduction of perturbation signals

1. Reduction of offset, drift, and noise

Experimentally we found that the residual field in the chamber is very sensitive to weak currents applied to the coil system (current sensitivity). A current I around 1 mA in the coils results in a remaining residual field shift of $\Delta|\boldsymbol{B}_r|=27$ pT in the center of the chamber. Such a current correspond to an input voltage $V_{\text{in}}=15$ μV (see Fig. 14) for the power amplifier (conversion factor of the power amplifier: 64 A/V). Due to the 20 dB attenuation, the amplitude of the DAC signal has to be $10V_{\text{in}}$. We found that the noisy digital ground of the PC, the resolution of the signal forming DAC, and the stability of the gradient power amplifier produce such signals. Thus, they had to be reduced. On the other hand the current amplitude we apply to generate the field H to demagnetize the BMSR-2 ranges from a peak value of 70 A down to a few microamperes. We utilize a 16 bit DAC (15 bit resolution and one polarity bit) which results theoretically in a current resolution of around 2 mA (15 bit). Due to the integral nonlinearities of about 0.5 LSB (least significant bit) at zero crossing a dc output current of about 2.7 mA for the power amplifier was measured. The user's manual of the gradient power amplifier specifies the peak-to-peak noise in the 0.1–1 Hz range with less than 6 mA. We measured drift peak amplitudes less than 0.5 mA and an offset of several microamperes.

To reduce the reproducibility $\sigma(|\boldsymbol{B}_r|)$, these erroneous signals must be reduced or eliminated. For this reason, the MRI power stage was extended by galvanic isolation both at its input and output [galvanic isolation primary (GIP) and galvanic isolation secondary (GIS) see Fig. 14] to eliminate offsets and drifts. Additional filters bandlimit transient pulses and noise (see Fig. 14) and shape the transfer characteristic around the frequency applied for demagnetization.

We measured the transfer function with a floating spectrum analyzer (HP-35670) for the whole signal chain $V_{\text{out}}/V_{\text{in}}$, which is depicted in Fig. 15 expressed as I_s/I_p in dB. $V_{\text{out}}/V_{\text{in}}$ is related to I_s/I_p, as follows:

$$20\log\left(\frac{I_s}{I_p}\right)=20\log\left(\frac{V_{\text{out}}}{V_{\text{in}}}\right)-C, \tag{31}$$

whereby C is a constant expressed in decibels, incorporating the voltage to current conversion factor of the gradient power amplifier and the value of the current measurement resistor replacing Z_L.

To design and improve conventional demagnetization equipment its transfer characteristic should be similar to Fig. 15.

2. Reduction of transient pulses

The effect of a bipolar transient pulse on the residual magnetic field was investigated using the static hysteretic model from above (see Fig. 2). An exemplary bipolar transient pulse and its effect on the residual magnetic field are depicted in Fig. 16, assuming a nonideal demagnetization resulting in a B_{r0}. The transient pulses with randomly distributed amplitudes which occur at the end of the demagnetization process have two origins. First, to deliver high currents into the load, the power amplifier generates high voltage. Therefore each output branch is floating 200 V_{dc} above ground. Switching off the amplifier results in a transient pulse current having a peak amplitude larger than 10 mA. The origin of this pulse lies in the slightly asynchronous reduction of the high voltage in the two output branches. The peak value of the amplitude varies statistically with every shutdown event. Second, the power amplifier operates in the

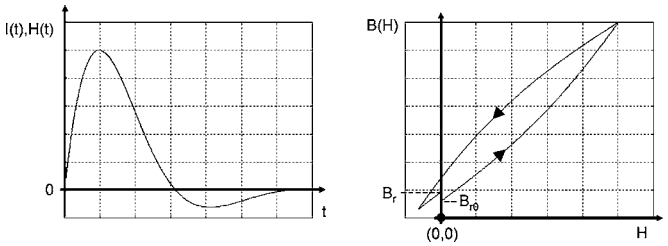

FIG. 16. Effect of a bipolar transient pulse after the demagnetization process on the residual magnetic field B_r using our static model. B_{r0}, residual field after demagnetization.

current mode; hence it behaves like a voltage controlled current source. A rapid load change from a finite value to infinity impedance forces the output voltage to its boundary. This reaction generates a peak current which is capacitive coupled into the load via the converter and the open switches (see Fig. 14). Due to the current sensitivity this leads to a lack of reproducibility. To reduce the effects of such transient pulses we implemented a substitute load Z_S which is switched in parallel to the impedance Z_L of the chamber and the isolated power stage before the connection between the Z_L and the amplifier is broken (see Fig. 14).

IV. RESULTS OF HARDWARE IMPROVEMENTS

This hardware upgrade strongly eliminates the integral drift and offset components. Due to the band limiting effect, the noise seen by the load is also reduced. A peak noise of 350 μA was measured at the output in the frequency range of 0.1–800 Hz, which corresponds to a peak input voltage of $V_{\text{in}}=11\mu$V. Comparing this value with the resolution of our 16 bit DAC (15 bit resolution and one polarity bit, 1 LSB $=300\ \mu$V) suggests the application of a DAC with higher resolution. All these implementations together gave us an improvement of $\sigma(|\boldsymbol{B}_r|)$ down to 110 pT, equal to a factor of 2.7. The bandpass characteristic of the converter (GIS) reduces the transient amplitude by a factor of 5. The implementation of a substitute load together with the switching paradigm reduces the transient current amplitude down to 10 μA, which is equal to an improvement factor of 1000 for the transient reduction. These additional implementations in combination with a small enough ΔH lead to a further improvement in reproducibility down to $\sigma(|\boldsymbol{B}_r|)=25$ pT in the center of the chamber. This results in an overall improvement factor of 12 for $\sigma(|\boldsymbol{B}_r|)$.

V. DISCUSSION

A. Improvement of demagnetization uncertainty

Having increased the reproducibility to such an extent makes small parameter variations of the demagnetization procedure measurable, which were hidden before by the effects of the perturbation signals. This improvement now enables the unaffected measurement of the decrease of $\sigma(|\boldsymbol{B}_r|)$ with decreasing $\Delta I(\sim\Delta H)$ down to a new boundary at $\Delta I=30$ ppm (see Fig. 17). This result supports the theoretical explanation given in Sec. II B about the interrelation between the improvement of reproducibility (variability) and decreasing step size. The measured data can be fitted by

$$\sigma(|\boldsymbol{B}_r|) = 1\times10^{-6}\Delta I^3 - 3\times10^{-4}\Delta I^2 + 0.0926\Delta I + 16.217, \tag{32}$$

with

$$\Delta I = \frac{I_0}{2N}.$$

This indicates that for $\Delta I\to 0$, $\sigma(|\boldsymbol{B}_r|)$ tends towards a fixed value. Our interpretation is that this boundary is mainly defined by the resolution of the DAC ($\Delta I=70\ \text{A}/2^{15}=2.13$ mA=31 ppm). From this we conclude that the outcome of demagnetization is achievable by variation of the parameters N and ω. Thus, the higher ω or N, the smaller the deviation from the ideal random orientation of the domains in the demagnetization direction. This therefore yields a finer fragmentation. The easiest way seems to increase ω while keeping T constant. In praxis ω is limited because of eddy-current effects in the ferromagnetic materials which reduce the penetration depth. With increasing ω the work necessary for a magnetization cycle increases due to the proportionality of the eddy-current power loss to ω^2. The area under a complete hysteretic cycle increases, i.e., H_c increases with ω. To reach the state of saturation requires a higher-field strength H and therefore a higher current. Therefore, the propitious way to lower dE/dt is to keep ω constant and increase T which leads to more cycles N.

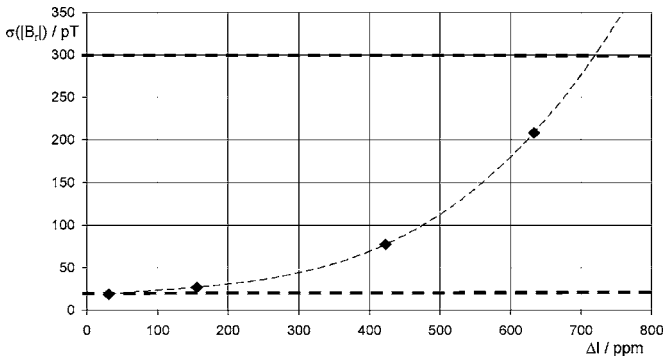

FIG. 17. Standard deviation $\sigma(|\boldsymbol{B}_r|)$ vs ΔI ($I_{\text{max peak}}=70$ A); numbers of measurements per ΔI $n=6$. Upper bold-type dotted line: Boundary of $\sigma(|\boldsymbol{B}_r|)$ with the variac based demagnetization unit. Lower bold-type dotted line: Boundary of $\sigma(|\boldsymbol{B}_r|)$ due to the digital resolution of the 16 bit DAC.

Our experimental outcomes reflect the results given by Ref. 20. This author shows the decreases of $\sigma(|\boldsymbol{B}_r|)$ with decreasing step size for two different linear decreasing demagnetization techniques. He also indicates that the residual magnetization is normally distributed. These results underline that they are valid for different linear decreasing demagnetization functions. It is interesting to note that the method introduced by Baynes[20] is used to demagnetize (deperming) naval vessels, which are large scale objects ($\gg$1 m) similar to a magnetically shielded room.

Assuming the normal distribution proposed by Ref. 20 we can state the distribution function $f(B)$ of the residual field of the BMSR-2 after demagnetization dependent on the applied step size ΔH, using Eq. (11) ($|B_r/B_S|$) for the mean value of B_r together with Eq. (32) [$\sigma(|\boldsymbol{B}_r|)$] for the standard deviation:

$$f(B) = \frac{1}{\sqrt{2\pi}\sigma(|\boldsymbol{B}_r|)} e^{-(1/2)((B-|\boldsymbol{B}_r|)^2/\sigma(|\boldsymbol{B}_r|)^2}. \tag{33}$$

B. Improvement of residual field gradient

In Fig. 1 we depict the increased noise level around 8 Hz which is caused by the movement of a SQUID sensor in the residual field gradient, induced by mechanical vibrations of the room. According to our theoretical predictions given in Sec. II and the experimental verification on a simple ferromagnetic structure (Fig. 9), we also expect a reduction of the

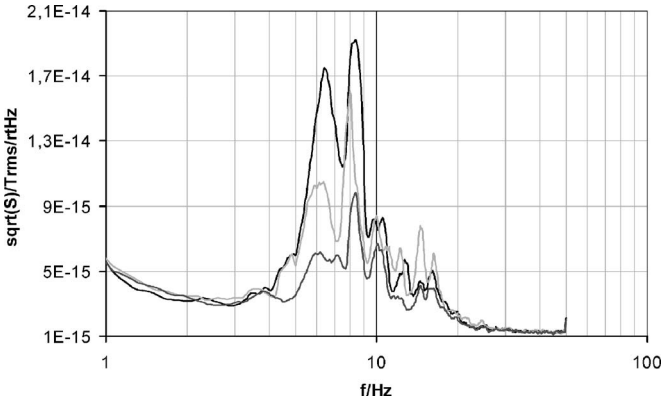

FIG. 18. Flux density noise measured inside the BMSR-2 for increasing number of oscillations N. Decrease of the averaged gradient (dB_z/dz) with decreasing step size. Highest noise level (darkest): State of the gradient after service works inside the chamber. Intermediate noise level (light gray): Demagnetization using 100 oscillations $(\Delta H/H_0=0.5\%)$. Lowest noise level (dark gray): Demagnetization using 5500 oscillations $(\Delta H/H_0=0.02\%)$; FFT with 30 averages.

fragmentation and therefore a smaller gradient in the BMSR-2. This should lead to a reduction of this perturbation signal. To evaluate this prediction we demagnetize the BMSR-2 gradually with decreasing step size using the linear decreasing envelope function. Figure 18 depicts the flux density noise created by mechanical vibrations in the z direction measured inside the BMSR-2 in the relevant frequency range of Fig. 1 with a spectrum analyzer.

Starting from a gradient caused by magnetizations due to service works (highest noise level) we applied our demagnetization function using 100 oscillations $(\Delta H/H_0=0.5\%$, intermediate noise level) and 5500 oscillations $(H/H_0=0.02\%$, lowest noise level). The application of 5500 oscillations reduces the flux density at 6 Hz by nearly a factor of 4, whereas 100 oscillations reach a factor below 2. Comparative measurements with our 304-SQUID-measurement system (Thiel *et al.* in 2005) showed that the local measurement, depicted in Fig. 18, is representative.

VI. SUMMARY

For high resolution biomagnetic measurements it is essential to offer a reproducible low residual field with a low gradient inside the magnetically shielded room. This can be achieved by proper demagnetization. High reproducibility can only be gained by elimination of the perturbation signals produced by the demagnetization equipment. We demonstrated how conventional demagnetization equipment should be improved. Subsequential parameter variation of the demagnetization function can be applied for further improvement of reproducibility and reduction of residual magnetic field and field gradient. Applying the derived approximation formula for a linearly damped ac-demagnetization function, the number of oscillations N, which are required to reach a desired residual field $|\boldsymbol{B}_r|$ close to the walls of the magnetically shielded room, can be estimated.

Based on the physics of ferromagnetism we derived criteria which a demagnetization function should meet to give a low residual field and field gradient. Our theoretical considerations indicate that the provided energy for demagnetization should be distributed over the demagnetization interval in such a way that the energy change during the traversing of the region of irreversible processes is small and can be large in the region of reversible processes. This leads us to an adaptation of the envelope function for the excitation field $H(t)$ by utilizing the material characteristics, i.e., the initial curve. To gain the material characteristics we provide a measurement method. From this measurement it is possible to adapt the shape of the envelope function to account for the energetic needs of the individual domain processes. Evidence is provided that with the parameter dE/dt, which includes the information about the ferromagnetic structure [e.g., $B(H)$], a statement of the outcome of the demagnetization process can be gained. Nonetheless, dE/dt allows the theoretical comparison of different ac-demagnetization function and the optimization of the envelope function. The boundary of this optimization process is given on the one hand by the limiting physical processes which are interrelated with the variation of the different parameters incorporated by dE/dt, e.g., increased power losses with increasing frequency. On the other hand, the energetic step size could not be smaller than the noise level given by the thermal noise plus the noise of the system itself. At the moment, the application of these theoretical conclusions is restricted by the hardware limitations of the demagnetization equipment. Therefore, our experimental investigations were carried out by applying a linear decreasing envelope function, which in turn has the advantage of direct comparability to conventional demagnetization equipment. We are still working on the elimination of the observed hardware restrictions to carry out the experimentally comparison of the two different demagnetization functions, applied to the BMSR-2. Nonetheless, we did this experiment on a simpler structure of similar ferromagnetic material and found a remarkable decrease in the residual field after application of the new demagnetization functions, which supports the theoretical predictions.

The experimental evaluation of our theoretical predictions supports the practical relevance of our findings. So, all these investigations and results could be very helpful to enhance the quality of conventional demagnetization equipment and procedures. This, in turn, supports the reliability of biomagnetic measurements in a clinical setting where conventional magnetically shielded rooms are installed.

Applying our results establishes a versatile demagnetization unit and creates outstanding measurement conditions inside the Berlin magnetically shielded Room-2. A residual magnetic field of $|\boldsymbol{B}_r|=900$ pT in the center with a standard deviation of $\sigma(|\boldsymbol{B}_r|)=25$ pT was achieved.

ACKNOWLEDGMENTS

The authors are grateful to H. Koch, F. Seifert, and H. Rinneberg for helpful experimental support and critical remarks. Further, they wish to thank G. Wübbeler for initial calculations with the hysteretic model.

[1] R. H. Koch *et al.*, Appl. Phys. Lett. **63**, 403 (1993).
[2] M. Burghoff, T. H. Sander, A. Schnabel, D. Drung, L. Trahms, G. Curio, B. M. Mackert, Appl. Phys. Lett. **85** (2004).

[3] R. McDermott, A. H. Trabesinger, M. Mück, E. L. Hahn, A. Pines, J. Clarke, Science **295**, 2247 (2002).
[4] W. Weitschies, O. Kosch, H. Monnikes, and L. Trahms, **57**, 1210–1222 (2005).
[5] A. Schnabel, R. Klein, J. Bork, H. Nowak, V. Schulze, L. Trahms, Biomed. Tech. **45**, 91–92 (2000).
[6] J. Bork, H. D. Hahlbohm, R. Klein, and A. Schnabel, Biomag 2000, *Proceedings of the 12th International Conference on Biomagnetism, 2001*, pp. 970–973.
[7] A. Schnabel, M. Burghoff, S. Hartwig, F. Petsche, U. Steinhoff, D. Drung, and H. Koch, Neurology, Neurophysiology, and Neuroscience (NNN) **70** (2004).
[8] F. Thiel *et al.*, Biomed. Tech. **50**, 169 (2005).
[9] L. de Almeida, G. S. Deep, A. M. N. Lima, and H. Neff, Sba Controle and Automação **14**, 58–68 (2003).
[10] F. Kohlrausch, *Praktische Physik*, Vol. 3, p. 24, Auflage, S (B. G. Teubner, Stuttgart, 1996), p. 54.
[11] F. Thiel *et al.*, *Proceedings of the BMT 2006* [Biomed. Tech. 51, 77 (2006)].
[12] J. S. Urbach *et al.*, Phys. Rev. Lett. **75**, 4694 (1995).
[13] D. Jiles and D. Atherton, IEEE Trans. Magn. **19**, 2183–2185 (1983).
[14] G. Durin and S. Zapperi, cond-mat/0404512.
[15] R. M. Bozorth, *Ferromagnetism* (D. Van Nostrand, New York, 1951), p. 476.
[16] S. Chikazumi, *Physics of Magnetism* (Wiley, New York, 1964), p. 245.
[17] L. Callegaro, E. Puppin, and S. Ricci, J. Phys. D **90**, 2416–2421 (2001).
[18] L. Callegaro, E. Puppin, and M. Zani, J. Phys. D **36**, 2036–2040 (2003).
[19] O. Chubykalo-Fesenko and R. W. Chantrell, J. Appl. Phys. **97**, 10J315 (2005).
[20] T. M. Baynes, IEEE Trans. Magn. **38**, 1753 (2002).
[21] M. Burghoff, H. Schleyerbach, D. Drung, L. Trahms, and H. Koch, IEEE Trans. Appl. Supercond. **9**, 4069–4072 (1999).
[22] A. Schnabel, D. Drung, S. Knappe-Grüneberg, and M. Burghoff, Proceedings of the Biomag, 2006, pp. 245 and 307.
[23] *Magnetic Shielding* (Vacuumschmelze, Hanau, Germany, 1989), FS-MM9, Edition.
[24] D. Platzek, H. Nowak, F. Giessler, J. Rother, and M. Eiselt, Rev. Sci. Instrum. **70**, 2465–2470 (1999).
[25] D. Drung, Physica C **386**, 134–140 (2002).